Electronic Supplementary Material (ESI) for Journal of Materials Chemistry C.

Supplementary Files

Heterostructured Plasmonic Memristors with Tunable Opto-Synaptic Functionalities

Mohammad Karbalaei Akbari [a,b], Ranjith K. Ramachandran [b], Christophe Detavernier [b], Jie Hu [c], Joondong Kim[d], Francis Verpoort [a], Serge Zhuiykov [a, b]

[1]Centre for Environmental & Energy Research, Ghent University, Global Campus, 21985, Incheon, South Korea.

[b]Department of Solid State Sciences, Faculty of Science, Ghent University, 9000 Ghent, Belgium.

[c]Centre of Nano Energy and Devices, College of Information and computer, Taiyuan University, Shanxi, China

[d]Photoelectronic and Energy Device Application Lab, Multidisciplinary Core Institute for Future Energies, Incheon National University, Incheon, South Korea.

*Corresponding author. E-mail: Mohammad.akbari@ugent.be; Serge.Zhuiykov@ugent.be.

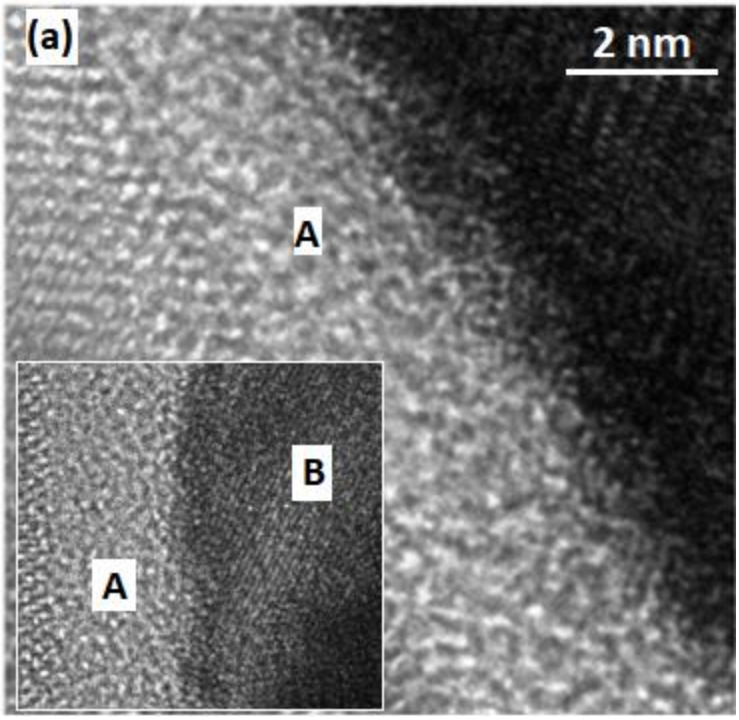

Supplementary Figure 1. The cross-sectional HRTEM image of (a) as-deposited In_2O_3 film. The [A] structure represents the In_2O_3 film. (Inset) Shows the cross-sectional HRTEM image of In_2O_3-TiO_2 heterostructured film where [A] represents the In_2O_3 film and [B] represents TiO_2 film.

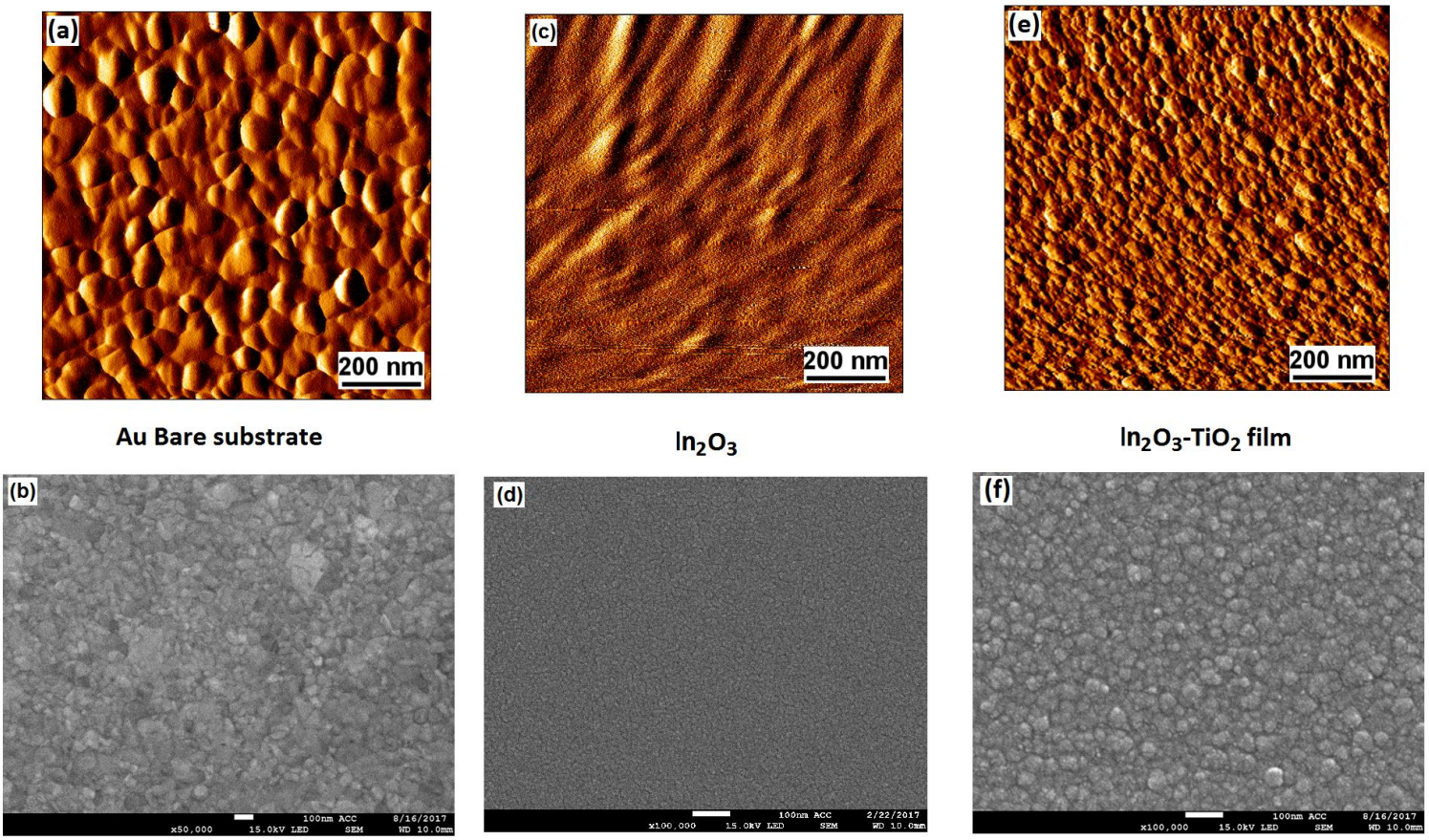

Supplementary Figure 2. Sequential stage of deposition of In_2O_3-TiO_2 heterostructured film. (a) AFM (top) and (b) FESEM image (down) of surface of bare Au film. The bare surface of Au substrate composed of granular Au structures (c) AFM image (top) and (d) FESEM image (down) of In_2O_3 film deposited on Au substrate. Ultra-thin In_2O_3-TiO_2 film covered the surface of granular Au film. The average roughness of In_2O_3 is 179 pm measured by AFM probe. (e) AFM image (top) and (d) FESEM image (down) of In_2O_3-TiO_2 heterostructured film. The In_2O_3-TiO_2 film uniformly covered the surface of granular Au film with vivid granular structure. The average roughness of TiO_2 is 78 nm measured by AFM probe.

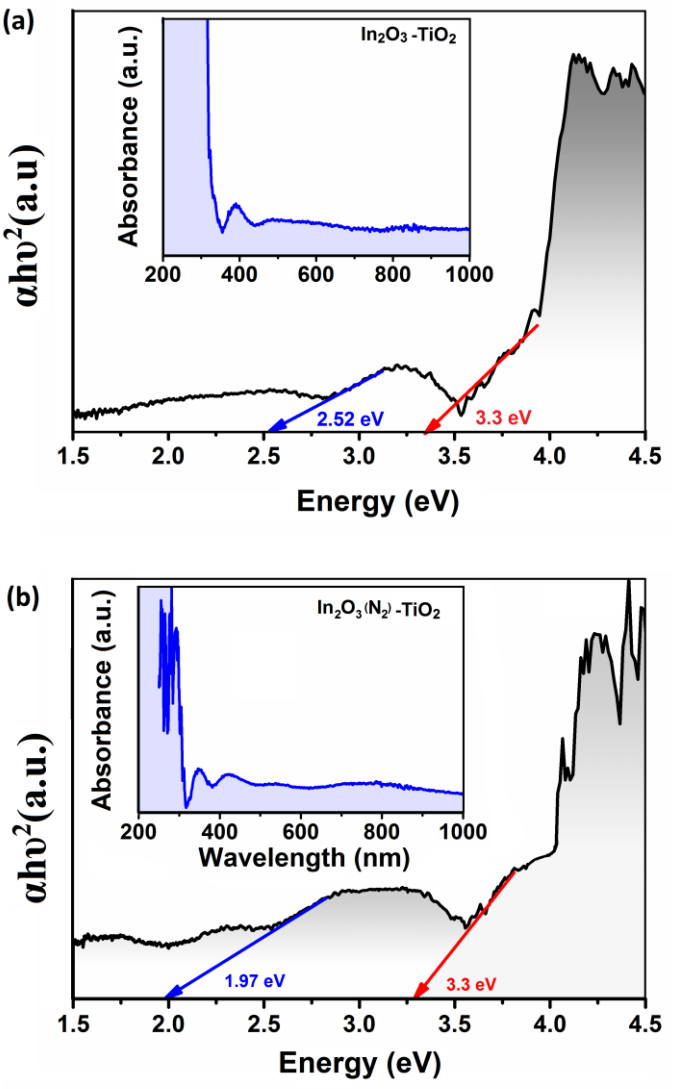

Supplementary Figure 3. The absorbance spectra of (a) In_2O_3-TiO_2 and (b) In_2O_3 (N_2)-TiO_2 samples accompanied by the calculated bandgap of heterostructured film.

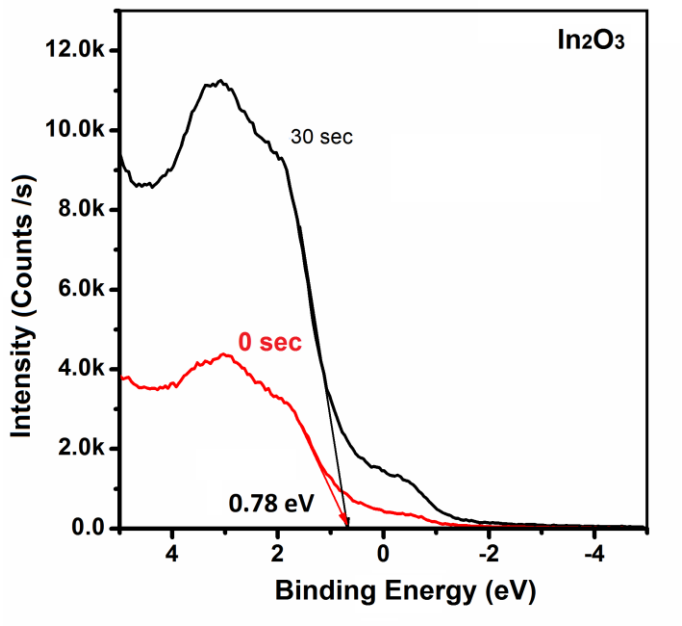

Supplementary Figure 4. The value of valence band maximum (VBM) of In_2O_3 film on surface and after 30 sec milling.

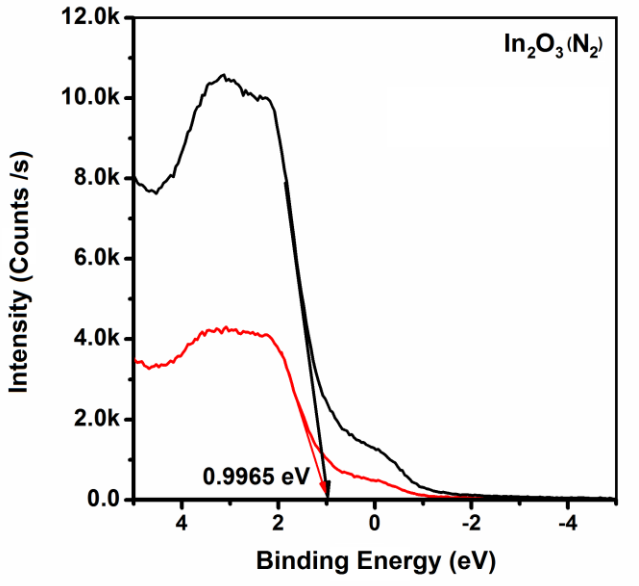

Supplementary Figure 5. The value of valence band maximum (VBM) of In_2O_3 (N_2) film on surface and after 30 sec milling.

Supplementary note 1:

Calculation of energy band alignment at semiconductor heterointerfaces

Based on Kraut's method, the valence band offset (VBO) can be extracted by following formula [1, 2]:

$$\Delta E_V = \left(E_{Ti\ 2P}^{TiO_2} - E_{VBM}^{TiO_2}\right) - \left(E_{In\ 3d}^{In_2O_3} - E_{VBM}^{In_2O_3}\right) - \left(E_{Ti\ 2P}^{TiO_2} - E_{In\ 3d}^{In_2O_3}\right) \quad \textbf{Formula 1}$$

$$\Delta E_V = \left(E_{Ti\ 2P}^{TiO_2} - E_{VBM}^{TiO_2}\right) - \left(E_{In\ 3d}^{In_2O_3(N2)} - E_{VBM}^{In_2O_3(N2)}\right) - \left(E_{Ti\ 2P}^{TiO_2} - E_{In\ 3d}^{In_2O_3(N2)}\right) \quad \textbf{Formula 2}$$

In which $E_{In\ 3d}^{In_2O_3}$ is core level (CL) spectra of In 3d, $E_{VBM}^{In_2O_3}$ is the valence band maximum (VBM) of In_2O_3, $E_{Ti\ 2P}^{TiO_2}$ is the CL of Ti 2P spectra, $E_{VBM}^{TiO_2}$ is the VBM of TiO_2. To calculate the VBM of In_2O_3 and TiO_2, the XPS spectra of In_2O_3, In_2O_3 (N_2) and TiO_2 were used. To describe the integrated band offsets of TiO_2-In_2O_3 heterojunction, the corresponding energy difference between conduction bands can be calculated from Formula 3 and 4:

$$\Delta E_C = E_{Bandgap}^{TiO_2} - E_{Bandgap}^{In_2O_3} - \Delta E_V \quad \textbf{Formula 3}$$

$$\Delta E_C = E_{Bandgap}^{TiO_2} - E_{Bandgap}^{In_2O_3(N2)} - \Delta E_V \quad \textbf{Formula 4}$$

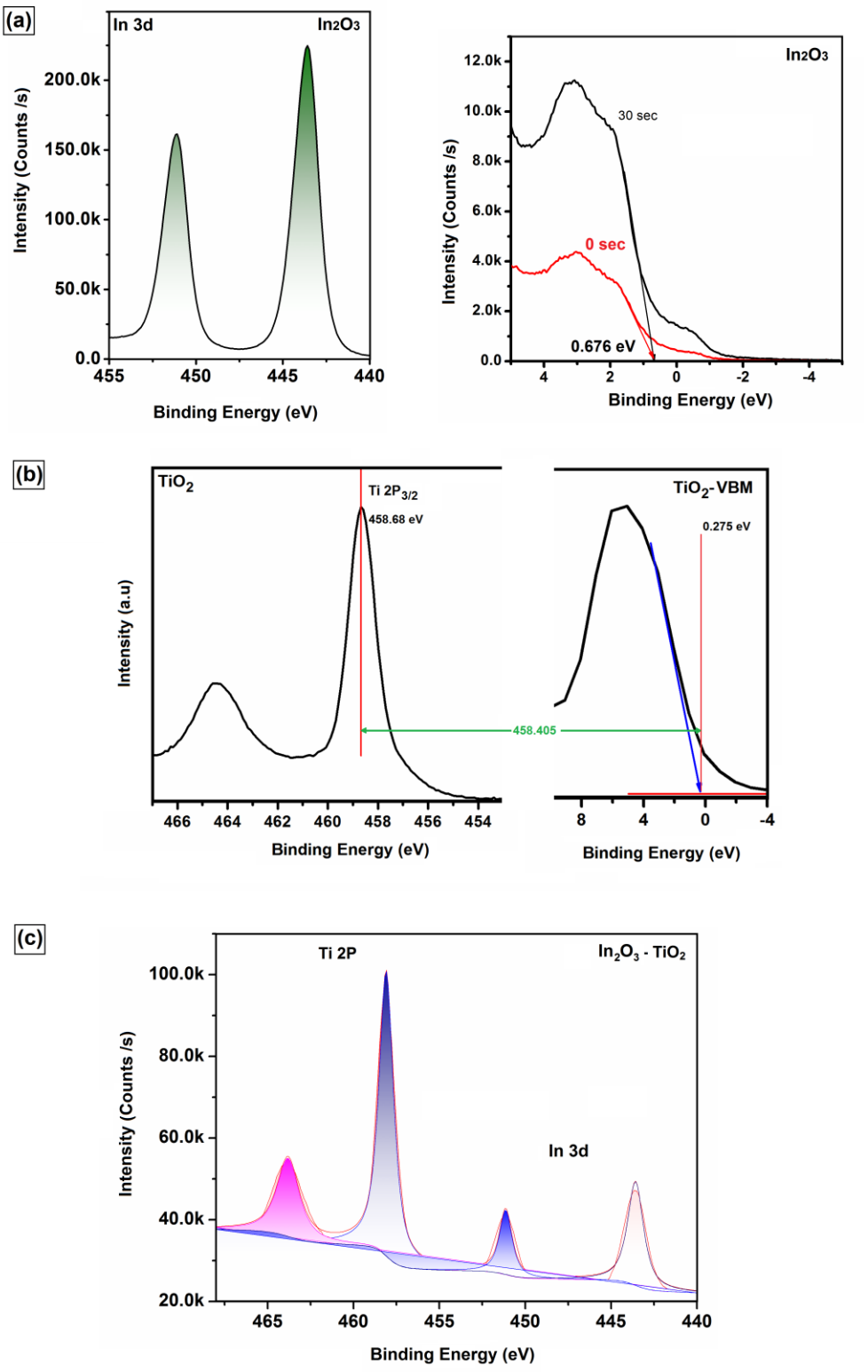

Supplementary Figure 6. XPS peak parameters for calculation of energy band alignment at In_2O_3-TiO_2 heterostructures.

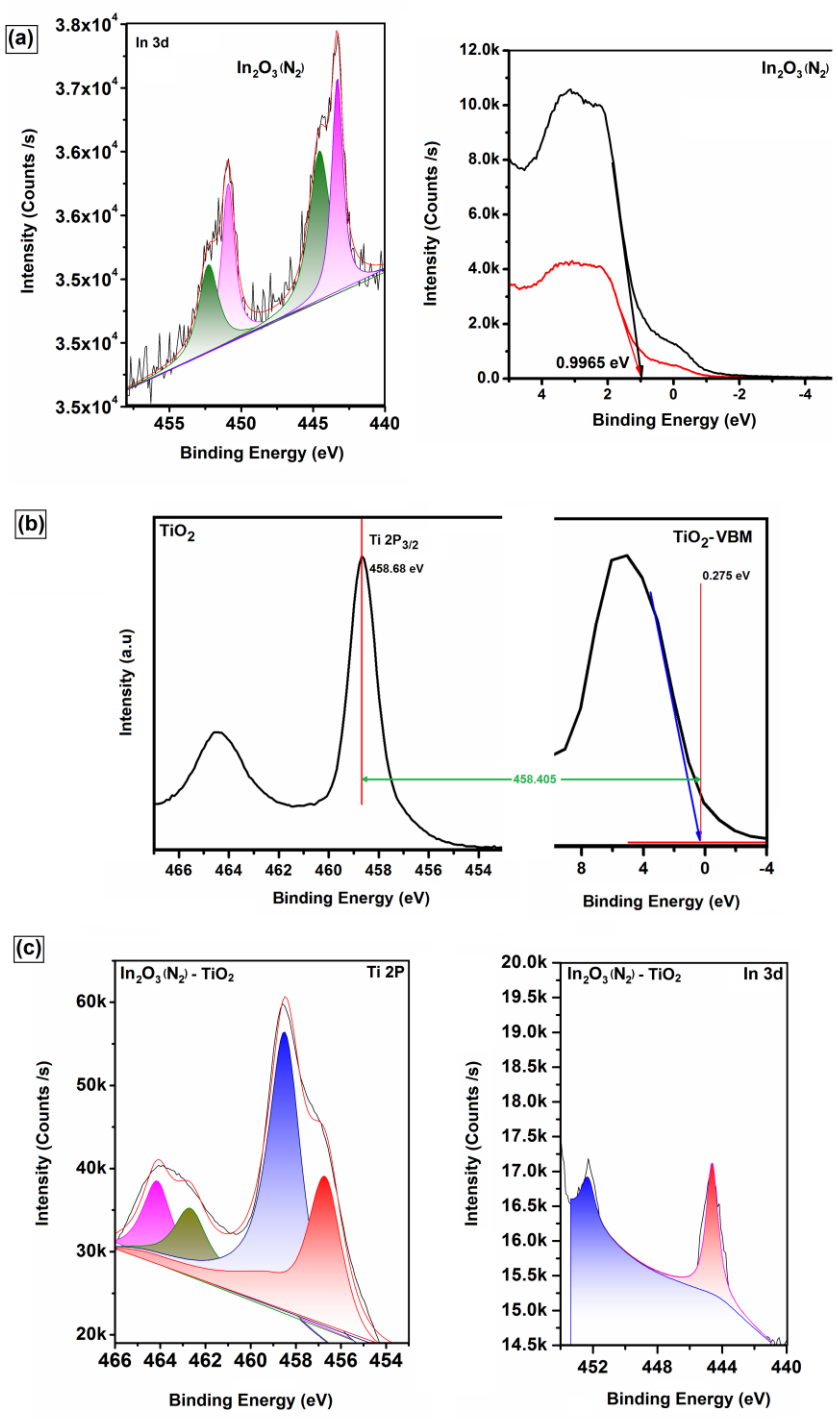

Supplementary Figure 7. XPS peak parameters for calculation of energy band alignment at In_2O_3 (N_2)-TiO_2 heterostructures.

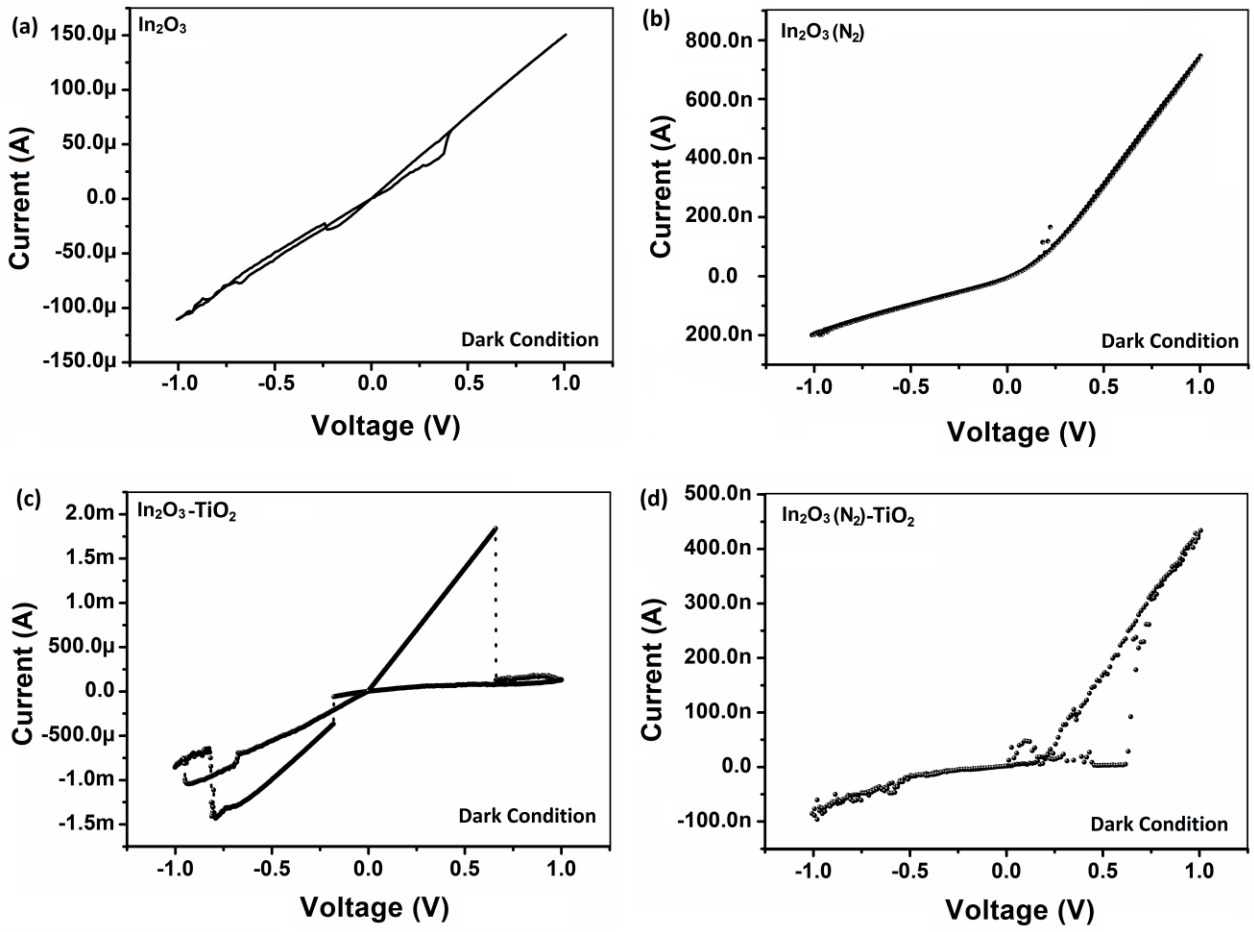

Supplementary Figure 8. The *I-V* cyclic curves of (a) In_2O_3, (b) In_2O_3 (N_2), (c) In_2O_3-TiO_2 and (d) In_2O_3 (N_2)-TiO_2 samples.

Supplementary Note 2. The Pt/In_2O_3/Au film demonstrated inconsiderable lope opening during the voltage sweeping from 0→1→0→-1→0 (Supplementary Figure 8a), which can be related to the restriction and ultra-low value of oxygen vacancies in 4.0 nm thick In_2O_3 film. This fragile loop openings were ultimately disappeared after RTA of 2D In_2O_3 film (Supplementary Figure 8b). The plausible explanation can be attributed the occupation of oxygen vacancies by nitrogen atoms. The most interesting properties of Pt/In_2O_3 (N_2)/Au device is its self-rectifying characteristics which are developed at the Au/In_2O_3 (N_2) heterointerface. The operational current of Pt/In_2O_3 (N_2)/Au memristor is also considerably decreased from Milli-Ampere ranges in the Pt/In_2O_3/Au device to several hundred nano-Amperes in the nitrogen incorporated 2D In_2O_3 film.

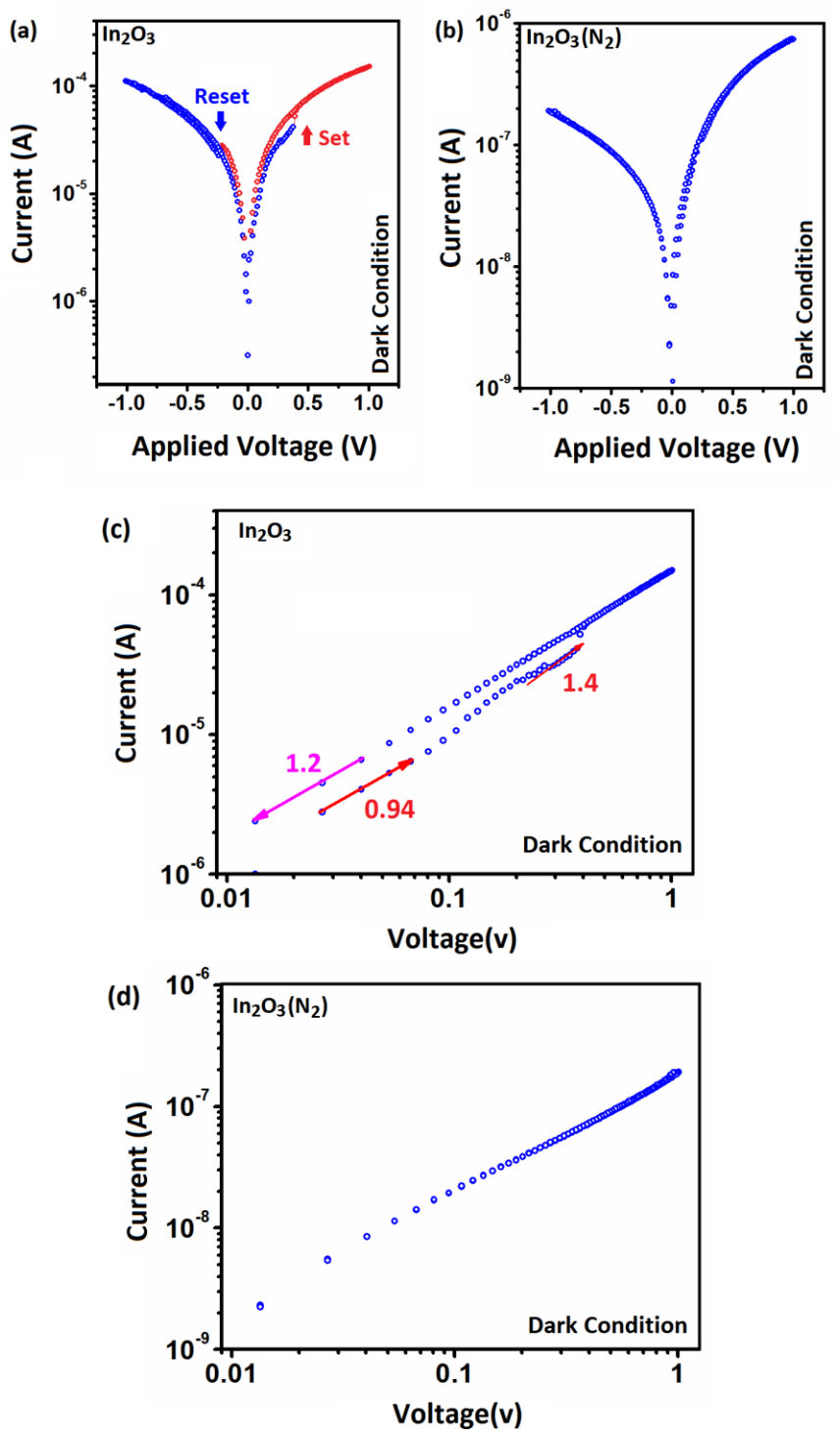

Supplementary Figure 9. The *log I-V* graphs of (a) In_2O_3 and (b) In_2O_3 (N_2) films, accompanied by *log I- log V* graphs of (c) In_2O_3 and (d) In_2O_3 (N_2) films.

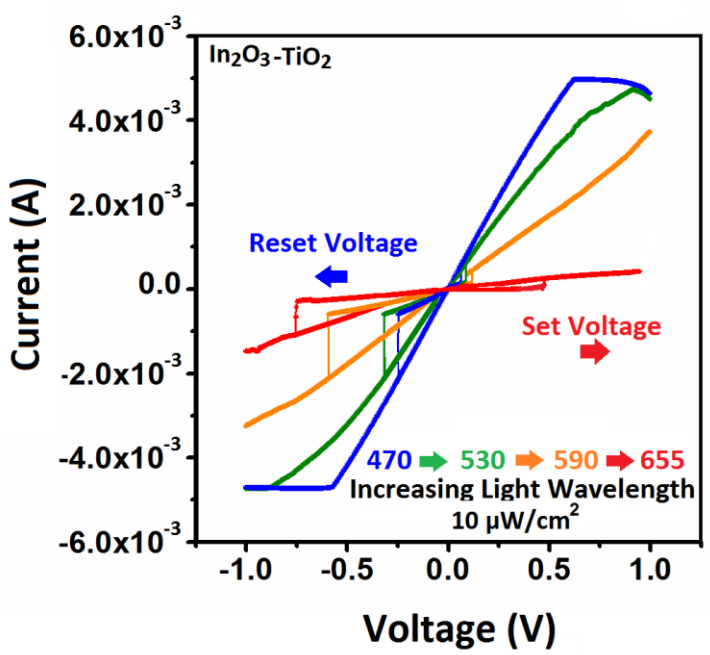

Supplementary Figure 10. The cyclic *I-V* curves of Au/In_2O_3-TiO_2/ITO memristors under illumination of 470 nm, 530 nm, 590 nm, and 655 nm visible lights.

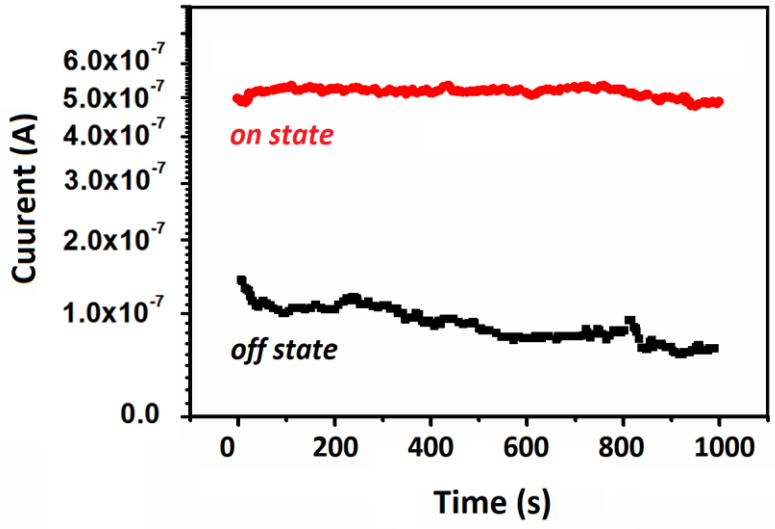

Supplementary Figure 11. The retention characteristics of Au/In_2O_3 (N_2)-TiO_2/ITO memristors under illumination of 470 nm with the light intensity of 10 μW/cm^2.

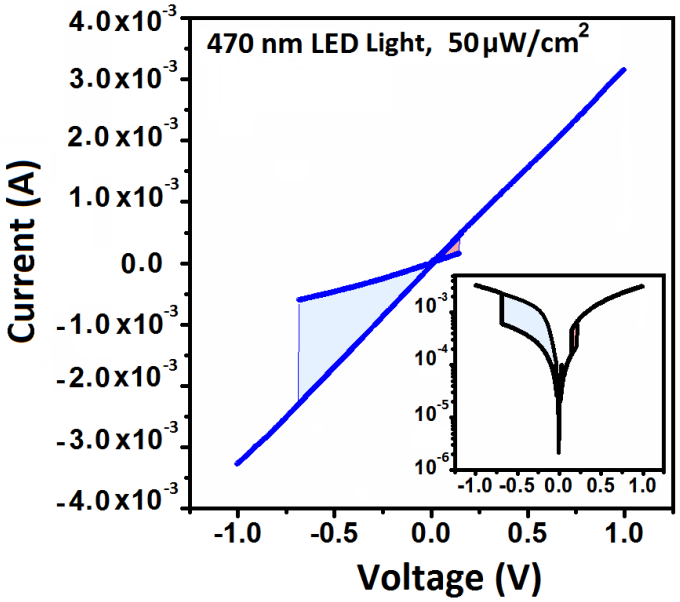

Supplementary Figure 12. The cyclic *I-V* curves of Au/$In_2O_3(N_2)$-TiO_2/ITO memristors under illumination of 470 nm visible lights at 50 μW/cm^2. The self-rectifying behaviour is deteriorated.

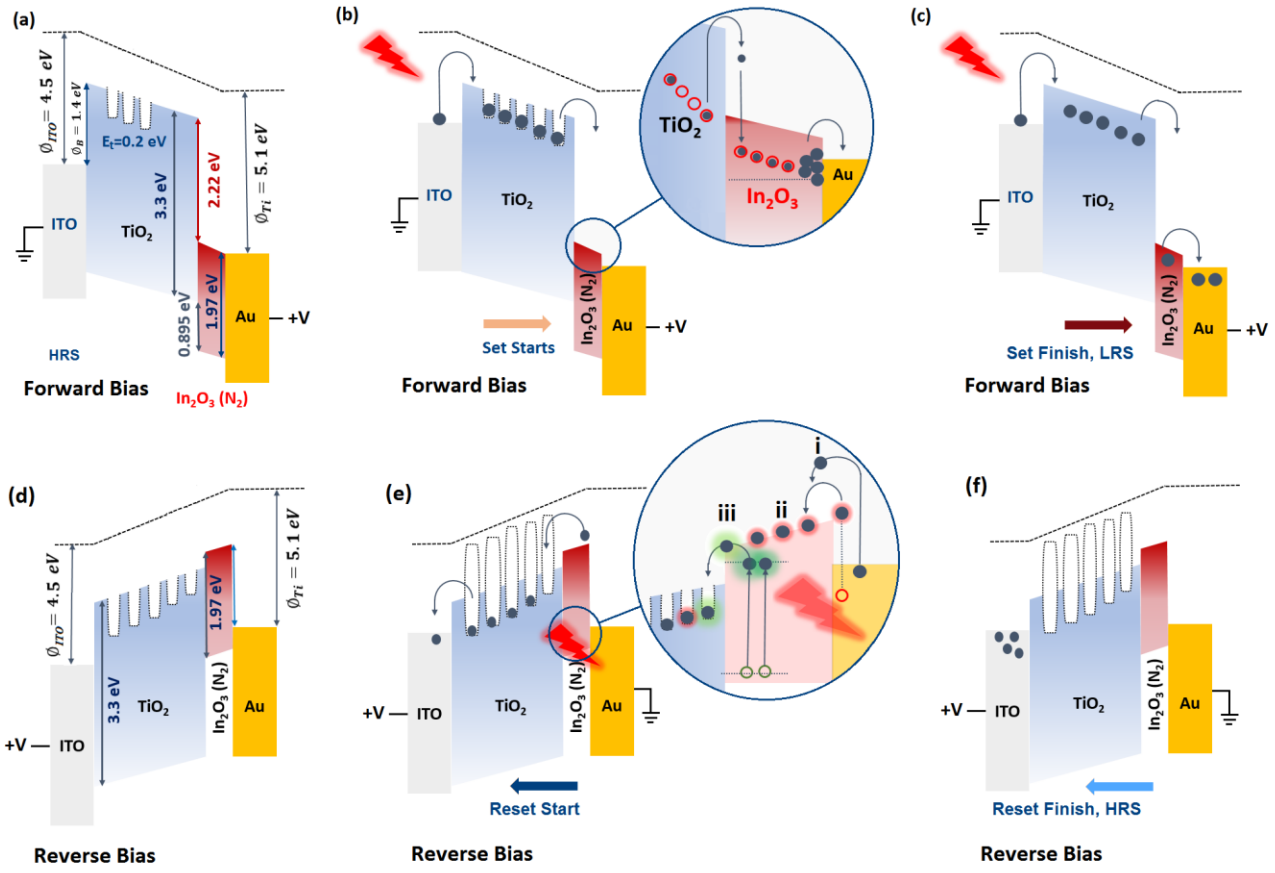

Supplementary Figure 13. The schematic of switching mechanisms of optical plasmonic memristors. (a) The energy band alignment diagram of the ITO/TiO_2-In_2O_3/Au device, (b) The illustration of charge trapping and detrapping process under visible light illumination when a positive bias voltage is applied. The trapped electrons are released and transmitted to Au electrodes and (c) LRS is achieved. (d) The schematic of energy band alignment at ITO/TiO_2-In_2O_3/Au device when the reverse bias voltage is applied on opto-memristor. (e) The plasmonic generated charge carriers and electrons should overcome a large Schottky barrier height (~ 2 eV) to occupy the trap sites and (f) finally restore the HRS mode.

Suplemnetray Note 3: The schematic energy band alignment of ITO/TiO_2-In_2O_3 (N_2)/Au heterointerfaces after the thermal equilibrium is depicted in Supplementary Figure 13a. It is assumed that the work function of ITO and Au conductive channels are respectively 4.5 eV and 5.1 eV. The bandgap of In_2O_3 (N_2) and TiO_2 are 1.97 eV 3.3 eV, respectively. The AE_c *and* AE_v at the TiO_2-In_2O_3 (N_2) are respectively 3.89 eV and 2.2 eV. The charge trap centres in 2D TiO_2 film are located 0.2 eV below the TiO_2 conduction bands. Considering the AE_c of 2.2eV at the TiO_2-In_2O_3 (N_2) hetero-interfaces, the Ti associated trap energy levels are 2 eV in the upper level than conduction band of In_2O_3 (N_2) film. Considering the Schottky barrier height

at the heterointerfaces of Au and ITO electrodes with TiO_2 main semiconductor, it is quite reasonable that the carrier trapping at 2D TiO_2 film is primarily occurs through the exchange of electrons with ITO electrode under the forward bias voltage. However, the presence of significant number of trapping cites at the Au/In_2O_3 (N_2) heterointerfaces determined the resistance value and switching mechanism of memristor. Supplementary Figure 13b depicts the occupation of Ti trapping sites in TiO_2 film via transmitted electrons from the ITO electrode under the forward bias voltage. After saturation of trapping sites in TiO_2 films, charge carriers are transmitted into Au/In_2O_3 (N_2) heterointerfaces. Considering higher thickness of TiO_2 film (19.0 nm) compared with the thickness of In_2O_3 (4.0 nm), both *F-N* and *direct tunnelling* mechanism are expected to be responsible for charge transfer. By applying higher voltage the set process is finalized and device will stay in LRS state (Supplementary Figure 13b c).

In reverse bias voltage, the barrier height between Au/In_2O_3 (N_2) and TiO_2 film is too high (~1.97 eV), thus the current flow under the applied bias voltage through the tunnelling and thermionic emission (Supplementary Figure 12d). By the applying a positive reversed bias voltage on Au electrode, the plasmonic photogenerated charge carriers try to pass the high-height Schottky barrier between Au/In_2O_3 (N_2) and TiO_2 hetero-interfaces (Supplementary Figure 13e). This process can be longer and changed based on the operating bias voltage and the visible light intensity. In LRS state the high-height Schottky barrier induces *self-rectification* behavior, i.e. the injection of hot electrons from Au/In_2O_3 (N_2) interface into TiO_2 film is inconsiderable. However, once the stronger reverse voltage is applied on Au electrodes, the Fermi level of Au/In_2O_3 (N_2) film is pulled up above the trap levels in TiO_2 film and then it facilitates the restoration of HRS state (Supplementary Figure 13f).

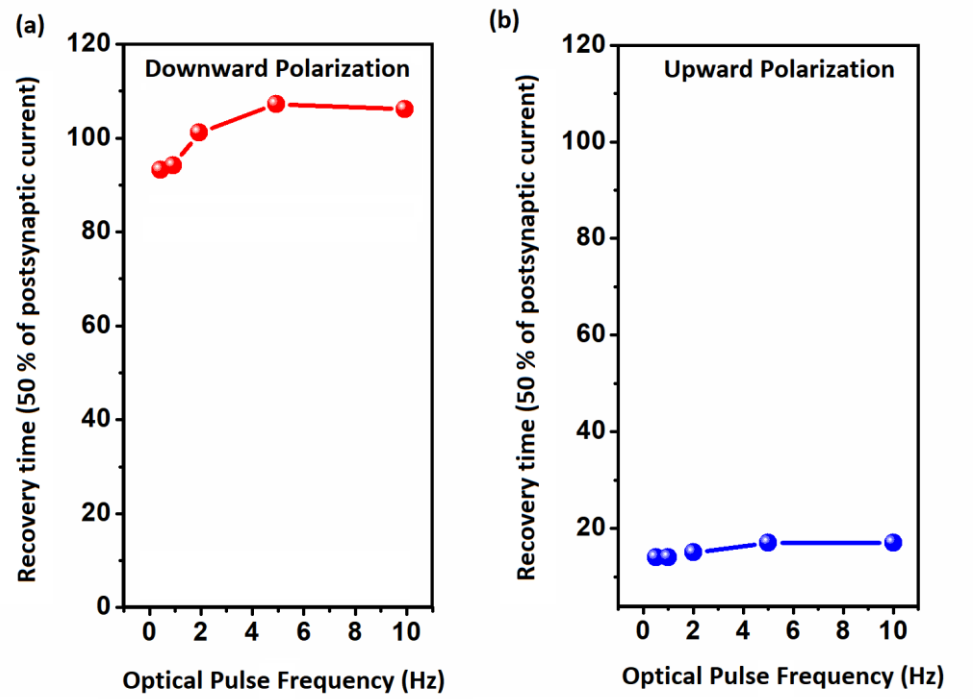

Supplementary Figure 14. The effect of light frequency on recombination time. The graph shows the required time for 50% retrieval of post-synaptic current.

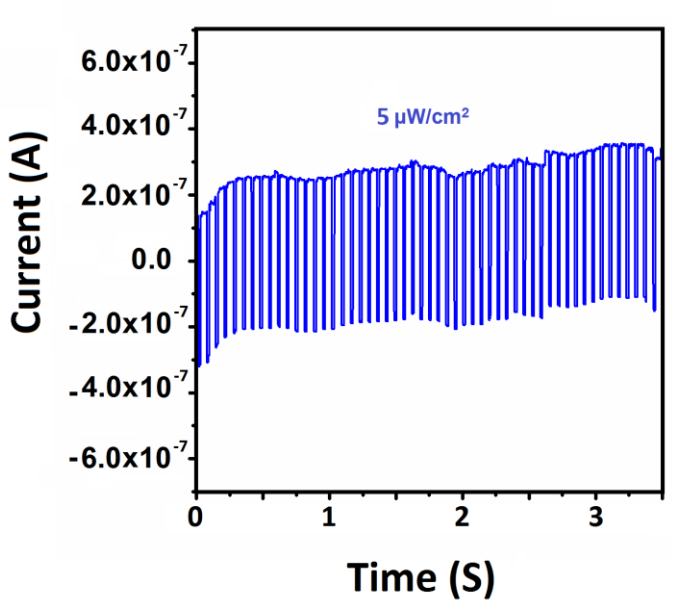

Supplementary Figure 15. The sequantial optical set (5 μW/cm^2) and voltaic reset (-0.1 V) of ITO/ TiO_2-In_2O_3 (N_2)/Au opto-synaptic device.

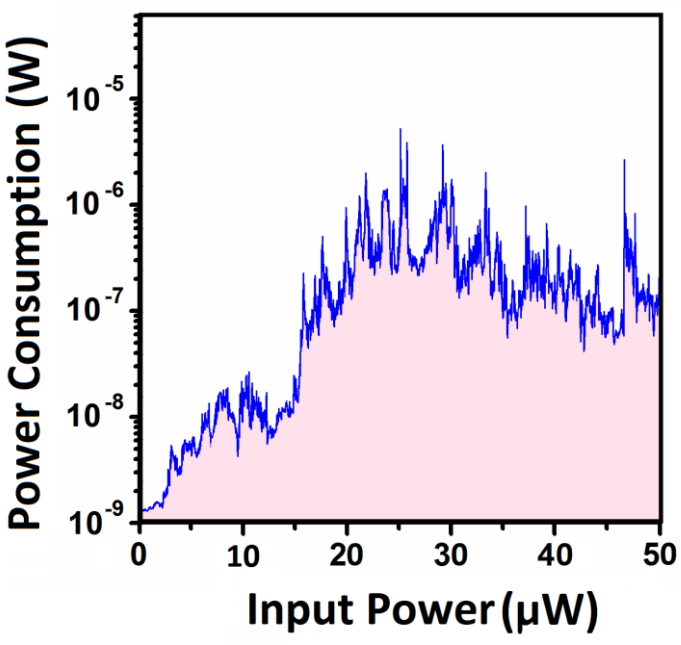

Supplementary Figure 16.The power consumption of ITO/ TiO_2-In_2O_3 (N_2)/Au opto-synaptic device vs. the input power of pulsed light.

References:

1. S. M. Sun, W. J. Liu, Y. P. Wang, Y. W. Huan, Q. Ma, B. Zhu, S. D. Wu, W. J. Yu, R. H. Horng, C. T. Xia, Q. Q. Sun, S. J. Ding, D. W. Zhang. Band alignment of In_2O_3/β-Ga_2O_3 interface determined by X-ray photoelectron spectroscopy. Appl. Phys. Lett. **113**, 031603 (2018) https://doi.org/10.1063/1.5038615
2. E. A. Kraut, R. W. Grant, J. R. Waldrop, S. P. Kowalczyk. Semiconductor core-level to valence-band maximum binding-energy differences: Precise determination by x-ray photoelectron spectroscopy. Phys. Rev. B. **28**, 1965 (1983) https://doi.org/10.1103/PhysRevB.28.1965